JOURNAL OF Applied Polymer SCIENCE

Fabrication of Transition-Metal-Doped Polypyrrole/Multiwalled Carbon Nanotubes Nanocomposites for Supercapacitor Applications

Saptarshi Dhibar, Sumanta Sahoo, C. K. Das
Materials Science Centre, Indian Institute of Technology, Kharagpur 721302, India
Correspondence to: C. K. Das (E-mail: chapal12@yahoo.co.in)

ABSTRACT: Copper chloride ($CuCl_2$)-doped polypyrrole (PPy)/multiwalled carbon nanotube (MWCNTs) nanocomposites were synthesized by an *in situ* oxidative polymerization method with ammonium persulfate as the oxidant in HCl medium and investigated as electrode materials for supercapacitors. The interaction of metal cations (Cu^{2+} ions) with PPy was confirmed by Fourier transform infrared spectroscopic analysis. The morphology of the nanocomposites was characterized by field emission scanning electron microscopy and high-resolution transmission electron microscopy. Electrochemical characterizations of the composites materials were carried out by a three-electrode probe method, where platinum and a saturated standard calomel electrode were used as the counter and reference electrodes, respectively. A 1*M* KCl solution was used as the electrolyte for all of the electrochemical characterizations. The transition-metal-ion doping enhanced the electrochemical properties of the conducting polymer. Among all of the composites, the $CuCl_2$-doped PPy/MWCNTs showed the highest specific capacitance value of 312 F/g at a 10 mV/s scan rate. © 2013 Wiley Periodicals, Inc. J. Appl. Polym. Sci. 130: 554–562, 2013

KEYWORDS: conducting polymers; electrochemistry; coatings; composites

Received 10 September 2012; accepted 11 February 2013; published online 20 March 2013
DOI: 10.1002/app.39176

INTRODUCTION

Supercapacitors, also known as *electric double-layer capacitors*, have played an important role in applications such as auxiliary power sources in combination with batteries in hybrid electric vehicles, backup power sources for computer memory, and short-term power sources for mobile electronic devices.[1–3] There are two types of electrochemical supercapacitors that are available on the basis of different mechanisms and charge storage. The first is the electric double-layer capacitor, which generally uses carbon-based active materials with high surface areas as electrodes. The accumulation of energy is done through the separation of electronic and ionic charges at the electrode–electrolyte interface. The second is known as a *pseudo-capacitor* or *redox supercapacitor;* it is actually based on redox active electrode materials such as metal oxides and conducting polymers.[4,5] Here, the accumulation of charge is done on the reversible surface through Faradic reactions.[2]

Conducting polymers, such as polypyrrole (PPy), polyaniline, polythiophene, and their derivatives, are an attractive class of electrode materials for supercapacitors with some important properties, including a high charge density, high doping–dedoping rates in charge–discharge processes, and simple synthesis via chemical or electrochemical methods.[6–8] The incorporation of carbon nanotubes (CNTs) as fillers into polymeric matrices increases the specific surface area and hence improves the electrical conductivity and mechanical properties.[9,10] Both single-walled CNTs and multiwalled carbon nanotubes (MWCNTs) have some unique properties, including a small size, high conductivity, high surface area, and enhanced stability; these enhance the electrochemical properties of the polymeric composite materials.[11–14] When conducting polymers are doped with transition-metal ions, such as Cu^{2+}, Zn^{2+}, and Fe^{2+}, the dopant ions act as redox active catalysts and improve the capacitance and thereby increase the energy density (E).

There have been many investigations on the electrochemical capacitance of PPy/MWCNTs nanocomposites by different synthetic techniques.[15–21] To the best of our knowledge, there are no scientific reports available on the investigation of electrochemical properties of copper chloride ($CuCl_2$)-doped PPy/MWCNTs nanocomposites. In this study, pure PPy, $CuCl_2$-doped PPy, and $CuCl_2$-doped PPy/MWCNTs nanocomposites were synthesized by *in situ* oxidative polymerization techniques with ammonium persulfate as the oxidant in HCl medium and investigated as electrode materials for supercapacitors. The electrochemical performances of the PPy nanocomposites were

studied by cyclic voltammetry (CV) and electrochemical impedance spectroscopy (EIS) with a three-electrode system.

EXPERIMENTAL

Materials Used

The pyrrole monomer used in this study was supplied by Merck (Drmstadt, Germany). Ammonium persulfate [$(NH_4)_2S_2O_8$] and HCl used in this study were supplied by Merck (Drmstadt, Germany). $CuCl_2$ used in this study was also supplied by Merck (Drmstadt, Germany). MWCNTs (MWCNT-1000) were obtained from IIjini Nanotechnology (South Korea). These MWCNTs had a diameter of 10–20 nm, a length of 20 μm, and an aspect ratio of about 1000. Cetyl trimethylammonium bromide was supplied by Loba Chemie Pvt., Ltd. (Mumbai, India).

Modification of the MWCNTs

The MWCNTs were modified in-house by thermal treatment to remove impurities such as metallic catalysts. For functionalization and chemical oxidation, the MWCNTs were subjected to an acid treatment.[22] Initially, 1 g of MWCNTs were mixed with a mixed acid solution containing 3 mol/L concentrated H_2SO_4 and 1 mol/L concentrated HNO_3 ($H_2SO_4/HNO_3 = 3:1$). At 1 : 100 weight ratios, the MWCNTs were mixed with the mixed acid. After the addition of the MWCNTs to the mixed acid, the whole solution was stirred at 60°C for 24 h. The mild acid treatment was not predicted to cause severe structural break of the MWCNTs.[23] The resulting mixture was then washed with distilled water until the pH of the solution became neutral. Then, the whole solution was centrifuged for 15 min at 3000 rpm to separate out the product. Finally, it was dried at 110°C for 24 h to yield carboxylic acid functionalized MWCNTs.

Synthesis of PPy

PPy was synthesized by chemical oxidative polymerization techniques in which $(NH_4)_2S_2O_8$ was used as an oxidant. First, 1 mL of pyrrole monomer was dissolved in 70 mL of a 1.5*M* HCl solution in a 200-mL beaker. In another breaker, 2 g of $(NH_4)_2S_2O_8$ was dissolved in 20 mL of deionized water. This $(NH_4)_2S_2O_8$ solution was then added dropwise to the pyrrole solution. The whole solution was then stirred at constant speed for 5 h at room temperature. After completion of the polymerization, the entire solution was filtered, washed with deionized water and ethanol several times, and dried at 60°C for 12 h.

Synthesis of Nanocomposites

For the synthesis of the nanocomposites, a typical *in situ* oxidative polymerization technique was used. First, in 150 mL of a 1.5*M* HCl solution, 1.24 g of cetyl trimethylammonium bromide and 60 mg of MWCNTs were added and sonicated for 45 min at room temperature. In another beaker, 1 mL of pyrrole was dissolved in 50 mL of a 1.5*M* HCl solution. Then, a 2 wt % $CuCl_2$ solution was added dropwise to the pyrrole solution and stirred for 15 min at room temperature. This $CuCl_2$-doped pyrrole solution was then added to the well-dispersed suspension of MWCNT solutions. After that, 60 mL of a 1.5*M* HCl containing 2.04 g of $(NH_4)_2S_2O_8$ was then added dropwise to the bulk solution and stirred for 5 h at room temperature. The solution was then kept at 1–5°C for 12 h for polymerization. After that, the precipitate was filtered, washed with distilled water and ethanol several times, and vacuum-dried at 70°C for 12 h to get the nanocomposites. The compositions of the nanocomposites are shown in Table I.

Table I. Compositions of the Composites

Sample code	PPy (wt %)	$CuCl_2$ (wt %)	MWCNTs (wt %)
PPy	100	0	0
PPy C2	98	2	0
PPy C2 CNTs	92	2	6

Characterization

Fourier Transform Infrared (FTIR) Analysis. FTIR analysis of the samples was carried out with a Nexus 870 FTIR instrument (Thermo Nicolet) in the range from 4000 to 400 cm^{-1}. The samples were prepared by the mixture of potassium bromide (KBr) and the nanocomposites at a weight ratio of 10 : 1; the mixture was pelletized to make the disks, and the disks were analyzed to obtain the spectra.

Field Emission Scanning Electron Microscopy (FESEM) Analysis. To investigate the surface morphology of the nanocomposites, a field emission scanning electron microscope (Carl Zeiss-SUPRA 40 FESEM, Oberkochen, Germany) was used. The powdered samples were put on carbon tape and then sputter-coated with gold. FESEM micrographs were taken at an operating voltage of 40 kV.

High-Resolution Transmission Electron Microscopy (HRTEM) Analysis. The doped PPy nanocomposites were analyzed by HRTEM (JEOL 2100, Tokyo, Japan) to check the uniformity of the coating of the Cu^{2+}-doped PPy in the MWCNTs. A small amount of sample was put in acetone and sonicated for 30 min in an ultrasonic bath. Then a drop of this dispersed solution was injected onto the copper grid for the HRTEM analysis.

Electrochemical Characterization. Electrochemical analyses, such as CV and EIS, were carried on a GAMRY instrument (750 mA and 2 V, Mumbai, India) with a three electrode system, where platinum and a saturated calomel electrode (SCE) were used as counter and reference electrodes, respectively. CV measurement was performed in a 1*M* KCl solution at different scan rates from 10 to 200 mV/s. The capacitances (C_{sp}'s) were calculated by the following equation.[24–26]

$$C_{sp} = (I_+ - I_-)/\nu m \quad (1)$$

where I_+ and I_- are the maximum currents in the positive and negative voltage scans, respectively; ν is the scan rate; and m is the mass of the composite materials. Impedance measurements were carried out for all of the composites in a 1*M* aqueous KCl solution by EIS. The electrode materials were prepared by the pressing of the composite materials at 10 MPa of pressure. The electrodes were used for electrochemical characterization without any polymer binder.

Electrical Conductivity Measurements. The electrical conductivity of the PPy, 2 wt% $CuCl_2$ doped PPy (PPy C2), and 2 wt% $CuCl_2$ doped PPy/MWCNT (PPy C2 CNT) nanocomposite were measured by conventional four-electrode probe methods

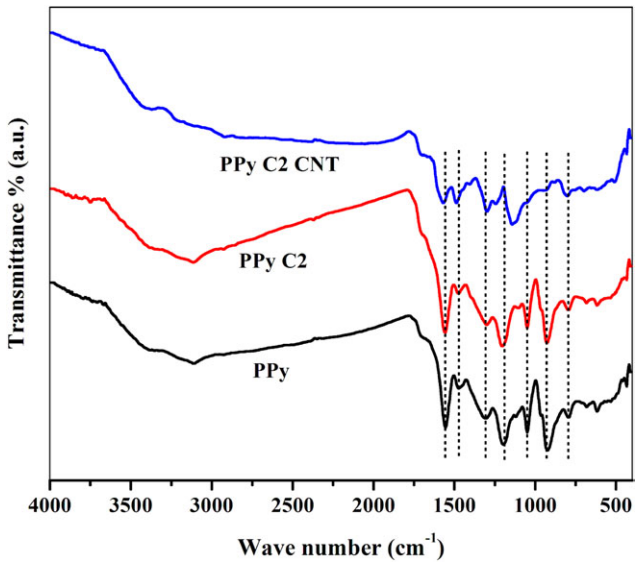

Figure 1. FTIR spectra of PPy, PPy C2, and PPy C2 CNT nanocomposites. [Color figure can be viewed in the online issue, which is available at wileyonlinelibrary.com.]

(Lakeshore resistivity and Hall measurement setup) with compressed pellets. All of the pellets were about 0.05 cm thick. The electrical conductivity was calculating with the following equation:

$$\rho = \pi t / \ln 2 (V/I)$$
$$= 4.53 \times t \times \text{Resistance}$$
$$\text{Conductivity } (\sigma; \text{S/cm}) = 1/\rho$$

where ρ is the resistivity (Ω cm), V is the measured voltage, I is the source current, and t is the thickness of the samples.

RESULTS AND DISCUSSION

FTIR Analysis

The FTIR spectra of the PPy, PPy C2, and PPy C2 CNT nanocomposite are presented in Figure 1. For all of the composite materials, a strong broad absorption band was found around 3395 cm^{-1}, which corresponded to the N—H stretching vibration, and the band at 3100 cm^{-1} was attributed to the aromatic C—H stretching vibrations. In PPy, the main characteristic peaks at 1555 and 1470 cm^{-1} were recognized as the pyrrole ring vibrations. The characteristic bands at 1306 and 1098 cm^{-1}

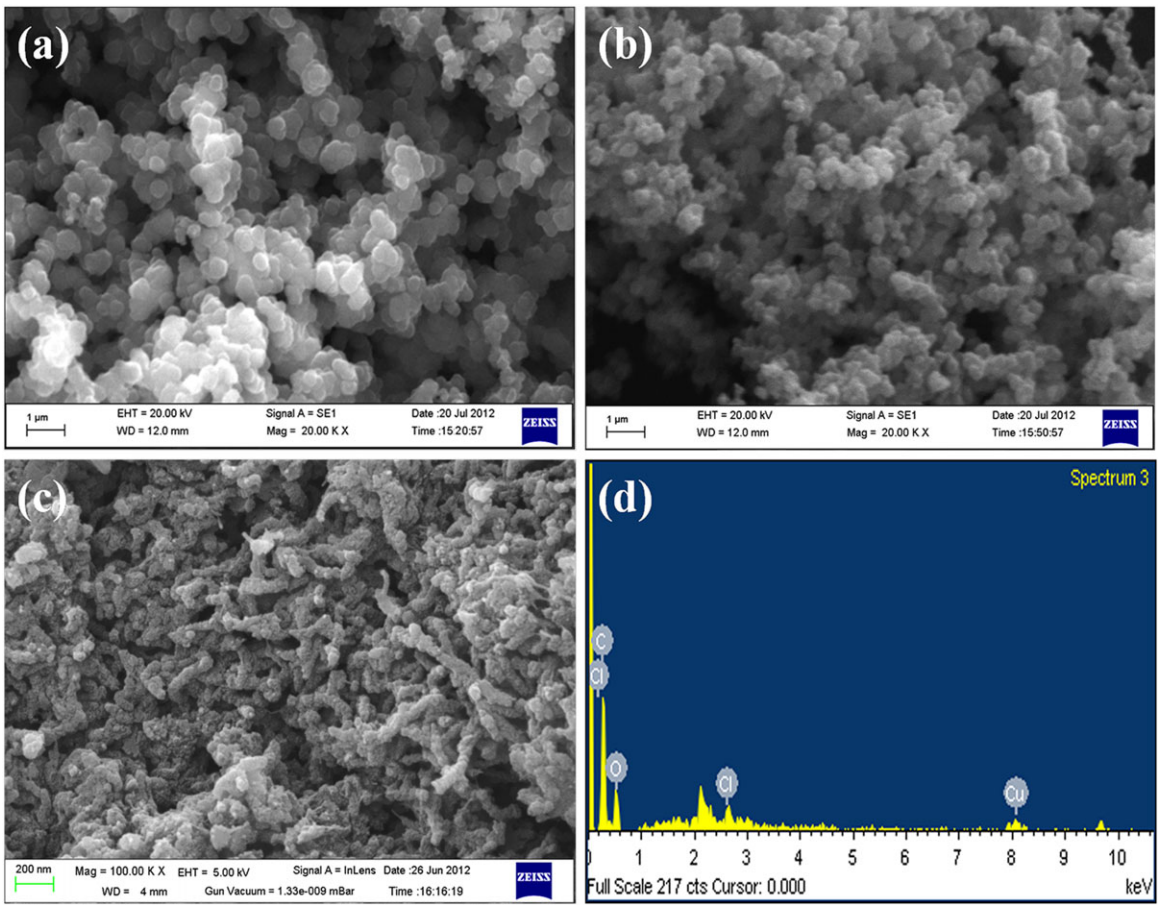

Figure 2. FESEM images of (a) PPy, (b) PPy C2, and (c) the PPy C2 CNT nanocomposites and (d) energy-dispersive X-ray spectroscopy spectrum of the PPy C2 CNT nanocomposites. [Color figure can be viewed in the online issue, which is available at wileyonlinelibrary.com.]

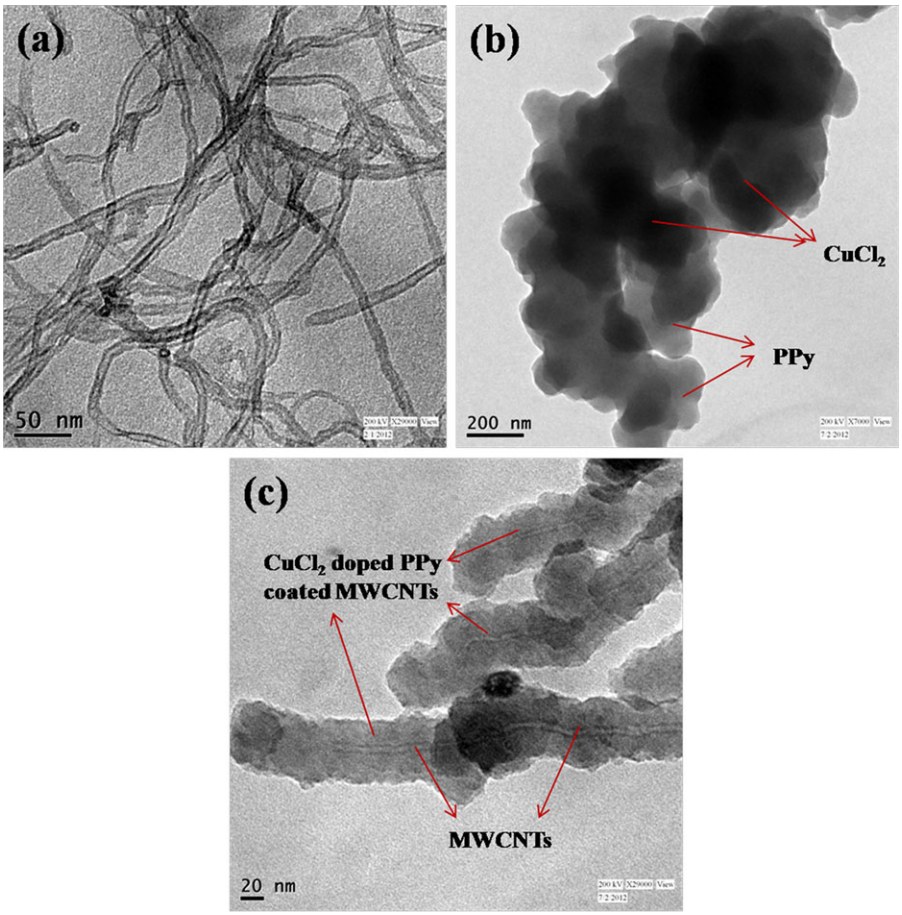

Figure 3. TEM images of the (a) acid-modified MWCNTs, (b) PPy C2, and (c) PPy C2 CNT nanocomposites. [Color figure can be viewed in the online issue, which is available at wileyonlinelibrary.com.]

were attributed to the =C—H in-plain deformation, and the band at 922 cm^{-1} was attributed to the =C—H out-of-plain vibrations. The characteristic band at 1196 cm^{-1} was attributed to C—N stretching vibrations. The results were in good agreement with the literature values.[27,28] It was observed from the FTIR spectra of PPy and PPy C2 that the characteristic peaks at 1555, 1470, and 1196 cm^{-1} shifted slightly to 1558, 1475, and 1202 cm^{-1}, respectively, in PPy C2. However, these characteristic peaks of PPy also shifted to 1568, 1487, and 1243 cm^{-1}, respectively, in PPy C2 CNT. This interesting phenomenon was attributed to the strong interaction between PPy and Cu^{2+} in both the PPy C2 and PPy C2 CNT nanocomposites.[29,30]

Surface Morphology Study

Figure 2 represents the FESEM images of the pure PPy, PPy C2, and PPy C2 CNT nanocomposites. As shown in Figure 2(a), PPy showed a granular morphology. However, after doping by $CuCl_2$, the grains were found to be much smaller than those of pure PPy [Figure 2(b)]. This decrease in the grain size was the result of maximum interaction between $CuCl_2$ and PPy. As shown in Figure 2(c), $CuCl_2$-doped PPy was uniformly coated on the MWCNT surfaces. The uniform coating suggested that the extreme interaction between the $CuCl_2$-doped PPy and the MWCNTs overcame van der Wall's interactions between the MWCNTs.[19] The energy-dispersive X-ray spectroscopy spectrum of the PPy C2 CNT nanocomposite confirmed the existence of copper and chlorine [Figure 2(d)].

HRTEM Analysis

The morphological characteristics of the $CuCl_2$-doped, PPy-coated MWCNTs nanocomposites was investigated by HRTEM analysis and are shown in Figure 3. Figure 3(a) shows the TEM image of the acid-modified MWCNTs, which shows that the average thickness of the MWCNTs was 15–25 nm. Figure 3(b) shows that the PPy particles were in an agglomerated form and were uniformly doped by $CuCl_2$. Figure 3(c) represents the TEM image of the PPy C2 CNTs, which shows that the $CuCl_2$-doped PPy particles were uniformly coated over the MWCNTs. The average diameter of the PPy C2 CNT nanocomposites was found to be 65–70 nm. The black portion on the TEM image indicates the presence of Cu in the PPy C2 CNT nanocomposite. This HRTEM study of PPy C2 CNT was well supported by FESEM analysis.

Electrochemical Characterization

To investigate the effect of Cu^{2+} doping on the electrochemical performance of the nanocomposites, CV analysis was carried out. The cyclic voltammograms of PPy, PPy C2, and PPy C2 CNT are shown in Figure 4. Their specific capacitance (C) value was calculated from the CV curve with eq. (1) and is

Applied Polymer SCIENCE

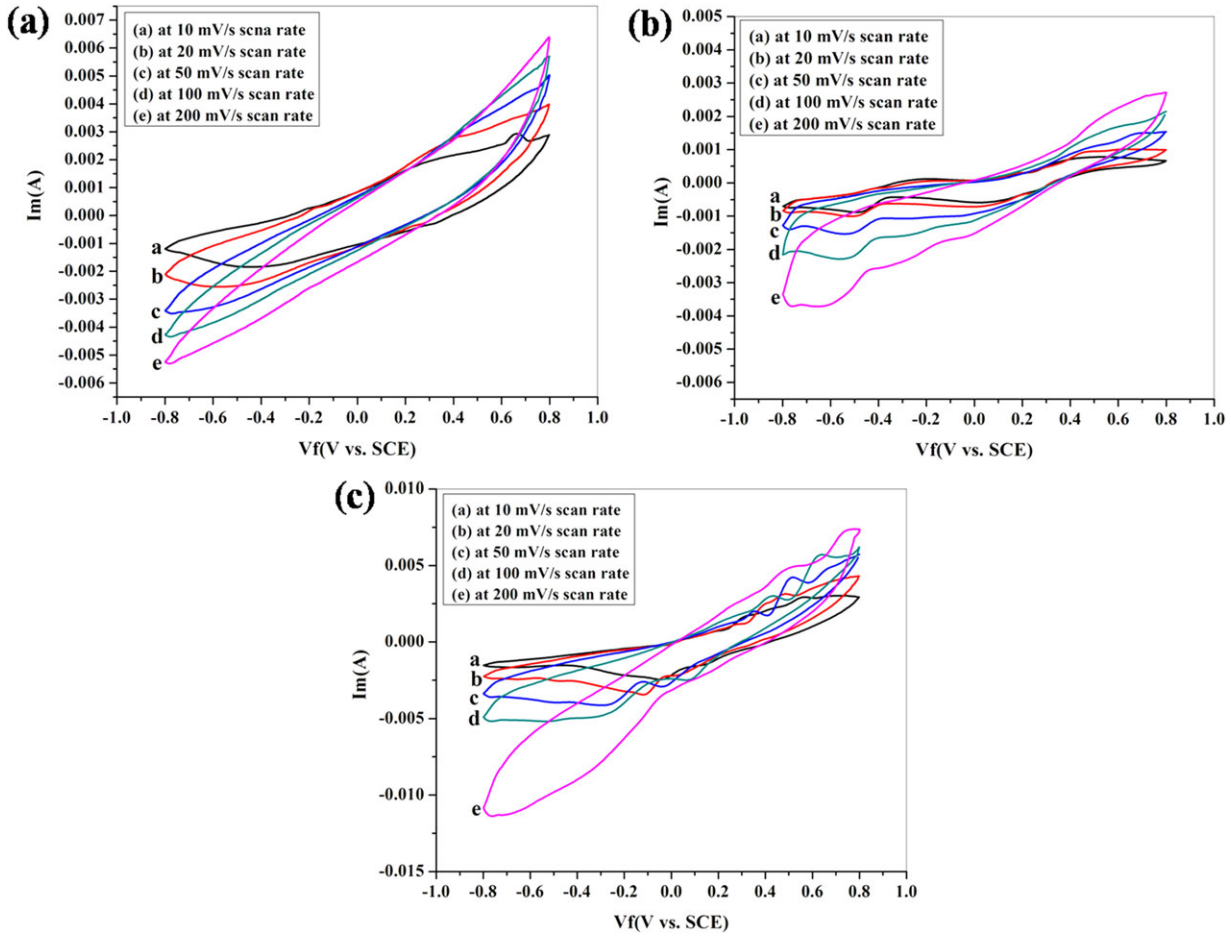

Figure 4. Cyclic voltammograms of (a) PPy, (2) PPy C2, and (c) the PPy C2 CNT nanocomposites. (Im indicates the current and Vf indicates the voltage in the CV curves). [Color figure can be viewed in the online issue, which is available at wileyonlinelibrary.com.]

summarized in Table II. The nanocomposites were examined within the applied voltage range of −0.8 to +0.8 V at 10, 20, 50, 100, and 200 mV/s scan rates. The negative and the positive current region in the CV curves indicate cathodic reduction and anodic oxidation, respectively. The nonrectangular shape of the CV curves signifies the redox behavior because of the occurrence of functional groups and/or a wide pore size distribution.

For PPy C2, at −0.6 V, one oxidation peak was observed [Figure 4(b)]. However, with a decrease in the scan rate, this oxidation peak shifted; this was mainly due to the resistance of the electrode. Again for the PPy C2 CNT nanocomposite, one oxidation peak was observed at −0.2 V. Furthermore, with an increase in the scan rate, positive shifts of the oxidation peaks were observed. Two reduction peaks were obtained at 0.35 and 0.52 V, and these reduction peaks were also shifted to a positive site, as shown in Figure 4(c). These shifting phenomenon of the oxidation and reduction peaks were due to electrode resistance.

Table II. *C* Values of the PPy, PPy C2, and PPy C2 CNT Nanocomposites at Different Scan Rates

Sample	10 mV/s	20 mV/s	50 mV/s	100 mV/s	200 mV/s
PPy	181	122	64	48	32
PPy C2	213	138	77	60	53
PPy C2 CNTs	312	219	112	65	56

We observed that among the PPy, PPy C2, and PPy C2 CNT nanocomposites, the PPy C2 CNTs achieved the highest *C* of 312 F/g at a 10 mV/s scan rate. The *C* values of PPy and PPy C2 were found to be 181 and 213 F/g, respectively. This increase in C for PPy C2 as compared to PPy may be due to the doping effect. The maximum C for PPy C2 CNT nanocomposites is caused by the uniform coating of CuCl2-doped PPy over MWCNTs: this was also revealed by the morphological studies. Furthermore, the doping effect of the Cu^{2+} ions on the polymer played an important role in the enhanced capacitance properties of the PPy C2 CNT nanocomposite. We observed that for all of the nanocomposites, with an increase in the scan rate, *C* decreased, as shown in Figure 5. This may have been due to the larger charge mobilization per unit time.

Karthikeyan et al.[15] reported Zn^{2+}-doped PPy/MWCNT composites synthesized by *in situ* oxidative polymerization and achieved the highest *C* of 327 F/g at a 10 mV/s scan rate. Sun

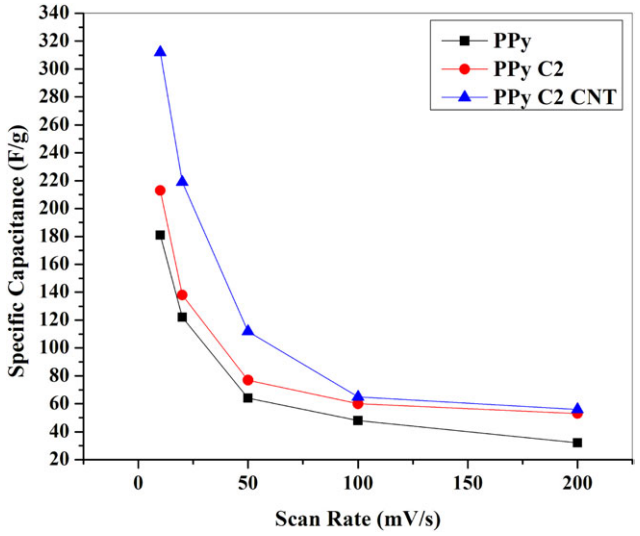

Figure 5. Plot of *C* versus the scan rate of PPy, PPy C2, and the PPy C2 CNT nanocomposites. [Color figure can be viewed in the online issue, which is available at wileyonlinelibrary.com.]

et al.[16] studied PPy/F–MWCNT composites prepared by electropolymerization techniques and achieved their highest *C* of 243 F/g at the scanning rate of 10 mV/s. Hughes et al.[17] studied the structure and capacitive properties of composite films prepared from catalytically grown MWCNTs and PPy composites via an electrochemical route and found the highest *C* of 192 F/g. Paul et al.[18] studied PPy/MWCNT/CC composites synthesized by chemical oxidative polymerization techniques and obtained the highest *C* of 238 F/g at a scan rate of 1 mV/s. They also reported PPy/MWCNT composites having a highest *C* of 167.2 F/g.[19] Jurewicz et al.[20] reported PPy/MWCNT composites synthesized by electrochemical polymerization techniques and achieved maximum *C* of 163 F/g at a 2 mV/s scan rate. Du et al.[21] reported the synthesis of PPy/CNT composites, which showed a *C* of 154.5 F/g.[21] A comparative study of these *C* values with our findings are summarized in Table III. In our study,

Table III. Comparative Study of the *C* Values of Different Nanocomposites

Composite	*C*	Reference
Zn^{2+}-doped PPy/MWCNTs	327 F/g	15
PPy/F-MWCNTs	243 F/g	16
MWCNTs/PPy (electrochemical route)	192 F/g	17
PPy/MWCNTs/CC	238 F/g	18
PPy/MWCNTs (oxidative polymerization techniques)	167.2 F/g	19
PPy/MWCNTs (electrochemical polymerization techniques)	163 F/g	20
PPy/CNTs	154.5 F/g	21
$CuCl_2$-doped PPy/MWCNTs	312 F/g	This study

Table IV. *E* Values of the PPy, PPy C2, and PPy C2 CNT Nanocomposites at Different Scan Rates

Sample	10 mV/s	20 mV/s	50 mV/s	100 mV/s	200 mV/s
PPy	64.35	43.37	22.75	17.06	11.37
PPy C2	75.73	49.06	27.37	21.33	18.84
PPy C2 CNTs	110.93	77.86	39.82	23.11	19.91

we got a *C* value of 312 F/g, which was better than the values reported in the literature previously.

The *E* values of the PPy, PPy C2, and PPy C2 CNT nanocomposite were determined by the following equation:

$$E = {}^1/_2(CV^2) \quad (2)$$

where *V* is the operating voltage. The power density (*P*) was also determined by the following equation:

$$P = E/t \quad (3)$$

where *t* is the time for completing the cycle (s).

The *E* and *P* values of the PPy, PPy C2, and PPy C2 CNT nanocomposites at various scan rates are summarized in Tables IV and V. It was observed that the PPy C2 CNT nanocomposites achieved a maximum *E* of 110.93 W h/kg at a 10 mV/s scan rate and a maximum *P* of 4479.75 W/kg at a 200 mV/s scan rate.

The variation of *C* with the number of cycles of the PPy, PPy C2, and PPy C2 CNT nanocomposite was done in a 1*M* KCl solution at a current density of 1 A/g and is shown in Figure 6. It was observed that after 1000 cycles, the *C* retention was 90% for the PPy C2 CNT nanocomposites; this indicated the long-term electrochemical stability of the composite. The *C* retention of PPy C2 CNT was higher than those of PPy and PPy C2, which were 80 and 84%, respectively, after 1000 cycles. The greater cyclic stability of the PPy C2 CNT nanocomposite compared to PPy and PPy C2 was due to the unique microstructure of the MWCNTs coated with $CuCl_2$-doped PPy.

EIS

A Nyquist plot is the most commonly employed plot for the analysis of EIS data. The interpretation of Nyquist diagrams is typically done by the fitting of the experimental impedance spectra to an electrical equivalent circuit. The fitted Nyquist

Table V. *P* Values of the PPy, PPy C2, and PPy C2 CNT Nanocomposites at Different Scan Rates

Sample	10 mV/s	20 mV/s	50 mV/s	100 mV/s	200 mV/s
PPy	723.93	975.82	1279.68	1919.25	2558.25
PPy C2	851.96	1103.85	1533.93	2399.62	4239
PPy C2 CNTs	1247.96	1751.85	2239.87	2599.87	4479.75

Applied Polymer SCIENCE

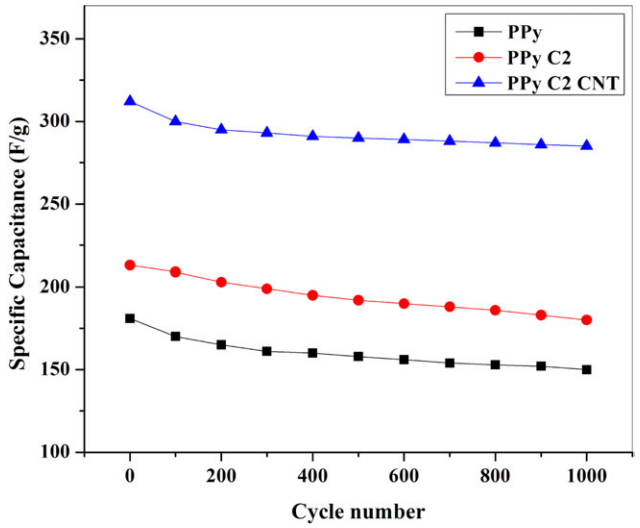

Figure 6. Plot of *C* versus the cycle number of PPy, PPy C2, and the PPy C2 CNT nanocomposite. [Color figure can be viewed in the online issue, which is available at wileyonlinelibrary.com.]

plots of the PPy, PPy C2, and PPy C2 CNT nanocomposites are shown in Figure 7. The area at higher frequencies indicated the electrolyte properties, and the area in the middle frequency was related to the electrode/electrolyte interface processes. The equivalent relaxation effect was signified by a semicircle, whose intersections at a higher frequency and middle frequency with the real axis were the solution resistance (R_s) and charge-transfer resistance (R_{ct}), respectively.

The appropriate equivalent circuit simulated with the experimental data is shown in Figure 8, and the fitting data of the PPy, PPy C2, and PPy C2 CNT nanocomposites are summarized in Table VI. The equivalent circuit used for this characterization was the standard circuit for the constant-phase element (CPE) with diffusion and has already been used by several research groups.[31,32] In real-world systems, capacitors are not perfect. These imperfect capacitors are signified as CPEs. The appearance of CPEs may occur because of (1) a distribution of the relaxation times as a result of inhomogeneity at the electrode/electrolyte interface, (2) dynamic disorder associated with diffusion, (3) porosity, and (4) the nature of the electrode.[33]

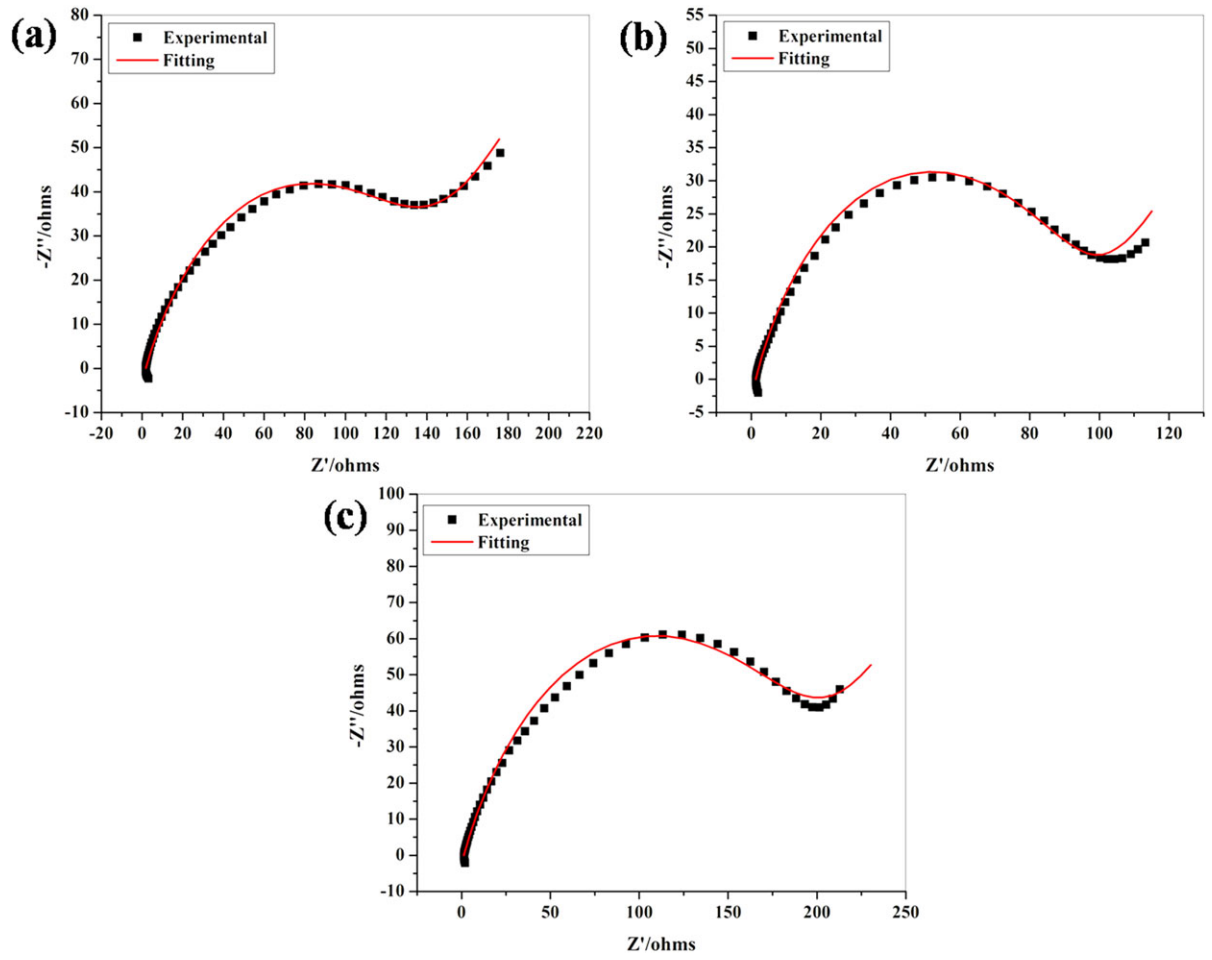

Figure 7. Nyquist plot of (a) PPy, (b) PPy C2, and (c) the PPy C2 CNT nanocomposites. Z′ indicates the real part and Z″ indicates imaginary part of the impedance. [Color figure can be viewed in the online issue, which is available at wileyonlinelibrary.com.]

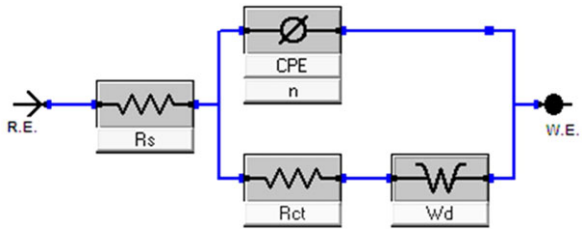

Figure 8. Equivalent electrical circuit used in the fitting data. R.E. = Reference Electrode, Wd = Warburg resistance, W. E. = Working Electrode. [Color figure can be viewed in the online issue, which is available at wileyonlinelibrary.com.]

R_s values of 1.78, 1.30, and 1.28 Ω were obtained for the PPy, PPy C2, and PPy C2 CNT nanocomposites, respectively. The lowest R_s value was found for the PPy C2 CNTs because of the enhanced electrical conductivity, which is an important factor in redox supercapacitors. The Warburg resistance (W) value was also lower for the PPy C2 CNT nanocomposites; this may have been because of the maximum charge delocalization of the Cu^{2+} ions. We got the highest frequency power n value ($n \approx 0.72$) for the PPy C2 CNT nanocomposites; this signified the porous nature of the electrode. The low impedance properties of the PPy C2 CNT nanocomposites indicated their potential for use as supercapacitor electrode materials.

Electrical Conductivity Study

The electrical properties of the nanocomposites were studied by a four-point probe measurement system and are summarized in Table VII. The introduction of MWCNTs into the doped composite enhanced the electrical properties because of the high surface area and large aspect ratio of MWCNTs. The highest electrical conductivity of 3.2 S/cm was found for the PPy C2 CNTs because of the uniform coating of $CuCl_2$-doped PPy on the CNT surface. The enhanced electrical conductivity of the composite made it superior for various device applications.

Table VI. Fitting Data for the Equivalent Circuit Elements of the PPy, PPy C2, and PPy C2 CNT Nanocomposites

Sample	R_s (Ω)	R_{ct} (Ω)	W ($S - s^{0.5}$) $\times 10^{-2}$	CPE ($S - s^n$) $\times 10^{-3}$	n
PPy	1.78	142.3	1.40	0.373	0.64
PPy C2	1.30	95.41	4.02	0.497	0.67
PPy C2 CNTs	1.28	200.2	2.10	0.401	0.72

Table VII. Electrical Conductivity Measurements

Sample	Thickness (cm)	Resistance (ohm)	ρ (Ω cm)	ρ (S/cm)
PPy	0.05	4.01	0.9	1.1
PPy C2	0.05	2.45	0.55	1.8
PPy C2 CNTs	0.05	1.38	0.31	3.2

CONCLUSIONS

The electrochemical performance of the $CuCl_2$-doped PPy-coated MWCNTs nanocomposites was investigated and compared with that of the undoped composites. The achievement of a high C for the doped composite was the result of the high charge delocalization on the polymer chains by the Cu^{2+} ions. Further, the $CuCl_2$-doped PPy-coated MWCNT nanocomposites showed the highest capacitance properties because of the uniform coating of $CuCl_2$-doped PPy on the MWCNT surfaces. Further, the fabrication of the nanocomposites and the experimental conditions will lead to superior application potential in supercapacitor and various innovative device applications.

ACKNOWLEDGMENTS

The authors thank the Defence Research & Development Organization, India, for financial support.

REFERENCES

1. Conway, B. E. *J. Electrochem. Soc.* **1991**, *138*, 1539.
2. Kotz, R.; Carlen, M. *Electrochim. Acta* **2000**, *45*, 2483.
3. Otero, T. F.; Cantero,I. *J. Power Sources* **1999**, 81–82, 838.
4. Conway, B. E.; Birss, V.; Wojtowicz, J. *J. Power Sources* **1997**, *66*, 1.
5. Girija, T. C.; Sangaranarayanan, M. V. *J. Power Sources* **2006**, *156*, 705.
6. Lin, Y. R.; Teng, H. *S. Carbon* **2003**, *41*, 2865.
7. Noh, K. A.; Kim, D. W.; Jin, C. S.; Shin, K. H.; Kim, J. H.; Ko, J. M. *J. Power Sources* **2003**, *124*, 593.
8. Park, J. H.; Ko, J. M.; Park, O. O.; Kim, D. W. *J. Power Sources* **2002**, *105*, 20.
9. Schadler, L. S.; Giannaris, S. C.; Ajayan, P. M. *Appl. Phys. Lett.* **1998**, *73*, 3842.
10. Qian, D.; Dickey, E. C.; Andrews, R.; Rantell, T. *Appl. Phys. Lett.* **2000**, *76*, 2868.
11. Du, C. S.; Yeh, J.; Pan, N. *Nanotechnology* **2005**, *16*, 350.
12. Ham, H. T.; Choi, Y. S.; Jeong, N.; Chung, I. *J. Polymer* **2005**, *46*, 6308.
13. Hughes, M.; Shaffer, M. S. P.; Renouf, A. C.; Singh, C.; Chen, G. Z.; Fray, J.; Windle, A. H. *Adv. Mater.* **2002**, *14*, 382.
14. Hughes, M.; Chen, G. Z.; Shaffer, M. S. P.; Fray, D. J.; Windle, A. H. *Chem. Mater.* **2002**, *14*, 1610.
15. Karthikeyan, G.; Das, C. K. *Macromol. Symp.* **2012**, *315*, 98.
16. Sun, X.; Xu, Y.; Wang, J.; Mao, S. *Int. J. Electrochem. Sci.* **2012**, *7*, 3205.
17. Hughes, M.; Chen, G. Z.; Shaffer, M. S. P.; Fray, D. J.; Windle, A. H. *Chem. Mater.* **2002**, *14*, 1610.
18. Paul, S.; Kim, J.-H.; Kim, D.-W. *J. Electrochem. Sci. Tech.* **2011**, *2*, 91.
19. Paul, S.; Lee, Y.-S.; Choi, J.-A.; King, Y. C.; Kim,D.-W. *Bull. Korean Chem. Soc.* **2010**, *31*, 1228.

20. Jurewicz, K.; Delpeux, S.; Bertagna, V.; Beguin, F.; Frackowiak, E. *Chem. Phys. Lett.* **2001**, *347*, 36.

21. Du, B.; Jiang, Q.; Zhao, X. F.; Huang, B.; Zhao, Y. *Mater. Sci. Forum* **2009**, *610–613*, 502.

22. Kumar, N. A.; Ganapathy, H. S.; Kim, J. S.; Jeong, Y. S.; Jeong, Y. T. *Eur. Polym. J.* **2008**, *44*, 579.

23. Kumar, N. A.; Bund, A.; Cho, B. G.; Lim, K. T.; Jeong, Y. T. *Nanotechnology* **2009**, *20*, 225608.

24. Sahoo, S.; Karthikeyan, G.; Nayak, G. C.; Das, C. K. *Synth. Met.* **2011**, *161*, 1713.

25. Dhibar, S.; Sahoo, S.; Das, C. K.; Singh, R. *J. Mater. Sci. Mater. Electron.* **2013**, *24*, 576.

26. Wang, J.; Xu, Y. L.; Sun, X. F.; Mao, S. C.; Xiao, F. *J. Electrochem. Soc.* **2007**, *154*, C445.

27. Liu, J.; Wan, M. *J. Polym. Sci. Part A: Polym. Chem.* **2001**, *39*, 997.

28. Mi, H.; Zhang, X.; Ye, X.; Yang, S. *J. Power Sources* **2008**, *176*, 403.

29. Maeda, S.; Armes, S. P. *Chem. Mater.* **1995**, *7*, 171.

30. Tu, J.; Li, N.; Yuan, Q.; Wang, R.; Geng, W.; Li, Y.; Zhang, T.; Li, X. *Synth. Met.* **2009**, *159*, 2469.

31. Bisquert, J.; Belmonte, G. G.; Bueno, P.; Longo, E. L.; Bulhoes, O. S. *J. Electroanal. Chem.* **1998**, *452*, 229.

32. Feliu, V.; Gonzalez, J. A.; Andrade, C.; Feliu, S. *Corros. Sci.* **1998**, *140*, 975.

33. Girifa, T. C.; Sangaranarayanan, M. V. *Synth. Met.* **2006**, *156*, 244.

34. Arami, H.; Mazloumi, M.; Khalifehzadeh, R.; Emami, S. H.; Sadrnezhaad, S. K. *Mater. Lett.* **2007**, *61*, 4412.